



# CO<sub>2</sub> capture by CaCO<sub>3</sub>-MgO and CeO<sub>2</sub>-MgO sorbents promoted by ternary alkali metal salts in a fixed bed reactor



Paula Teixeira <sup>\*</sup>, Patricia Correia, Carla I.C. Pinheiro

*Centro de Química Estrutural, Instituto de Molecular Sciences, Departamento de Engenharia Química, Instituto Superior Técnico/Universidade de Lisboa, Av. Rovisco Pais 1, Lisboa 1049-001, Portugal*

## ARTICLE INFO

**Keywords:**  
MgO sorbents  
CO<sub>2</sub> Capture  
Alkali metal salts  
Sol-gel synthesis  
Supported sorbents  
Fixed bed reactor

## ABSTRACT

MgO-based sorbents present a high theoretical CO<sub>2</sub> carrying capacity which make them promising materials for CO<sub>2</sub> capture at intermediate temperatures (200–400 °C). In this work, the MgO, CaCO<sub>3</sub>-MgO and CeO<sub>2</sub>-MgO sorbents were successfully synthesized by sol-gel technique. To enhance the CO<sub>2</sub> capture performance a eutectic ternary alkali metal salt mixture consisting of 15 % of NaNO<sub>3</sub>/KNO<sub>3</sub>/LiNO<sub>3</sub> (18/30/52) was added to the sorbents. The sorbents were tested in a fixed bed reactor unit along ten carbonation-calcination cycles, at 280 °C (25 % or 100 % of CO<sub>2</sub>) and 400 °C (100 % air), respectively. To identify textural, mineralogical, and morphological properties, the fresh and spent sorbents were characterized by N<sub>2</sub> adsorption, XRD and SEM techniques. The results show that the addition of Ca or Ce precursors enhance the stability of sorbents surface area along the carbonation-calcination cycles and improves the AMS dispersion, reducing their agglomeration and contributing to the enhancement of the MgO-based sorbents' CO<sub>2</sub> carrying capacity.

## 1. Introduction

The growth of industry and increasing energy consumption caused the gradual rise of the CO<sub>2</sub> levels in the atmosphere, reaching maximum values (>420 ppm) in 2023. Human activity-related CO<sub>2</sub> emissions are mostly originated from the energetic, industrial, and transportation sectors. Carbon capture, utilization, and storage (CCUS) has been considered, among other approaches, as a possible route to reduce the energetic and industrial sectors carbon footprint. Direct CO<sub>2</sub> capture (DCC) from air, is a complementary alternative to remove the CO<sub>2</sub> released from hard to abate sectors (e.g. transport). Although commercial CCUS deployment has been growing slowly, its impact on global CO<sub>2</sub> emissions is currently limited, despite its important role in mitigating climate change (Cavazos et al., 2023). The capacity of the world's power and industrial facilities to capture CO<sub>2</sub> was 40 Mt (IEA, 2020), in 2021, which only made up 0.12 % of the CO<sub>2</sub> emissions in the worldwide (Cavazos et al., 2023). The development of low cost, environmentally friendly and efficient CCUS technologies need to be leveraged to reach the target goal of net zero emissions by 2050, but according to the International Energy Agency (IEA) the CCUS capacity needs to increase to 7600 MtCO<sub>2</sub>/year (IEA, 2021). There are several technologies to capture CO<sub>2</sub>, including chemical absorption, membrane separation, adsorption,

and cryogenic CO<sub>2</sub> capture. Currently, the CO<sub>2</sub> absorption by liquid amines is the most developed and used technology in the industrial/energetic sectors, but it has problems related to the process high energy consumption, high sorbent cost, gas-liquid interfacial surface area and ineffective regeneration (Reddy et al., 2021). To overcome these limitations, the use of solid sorbents became a promising alternative. The operating range of solid sorbents can be based on their capture-regeneration temperature, i.e., low temperature sorbents (<200 °C), like zeolites, metal organic framework (MOF) and carbon-based sorbents, medium temperature sorbents (200–400 °C), like MgO-based and hydrotalcite like compounds, and high temperature sorbents (>400 °C) like Li/Na-based sorbents, CaO-based and SrO-based sorbents. Besides the CO<sub>2</sub> capture capacity, the trade-off between parameters like the cost production, stability and energy consumption for regeneration, is helpful for the sorbent's design and performance evaluation. Some of these sorbents are expensive (e.g. MOFs), moisture sensitive (e.g. zeolites), require a high regeneration temperature (e.g. CaO-based and SrO-based sorbents), or the maximum CO<sub>2</sub> adsorption is low (e.g. Li/Na-based sorbents, hydrotalcite). Another criterion is the sorbents' operating range since it can limit their application, i.e., can be used only in post- and/or pre-combustion conditions. MgO is a medium-temperature sorbent (200–400 °C), that in terms of carbon capture and storage (CCS)

\* Corresponding author.

E-mail address: [paula.teixeira@tecnico.ulisboa.pt](mailto:paula.teixeira@tecnico.ulisboa.pt) (P. Teixeira).

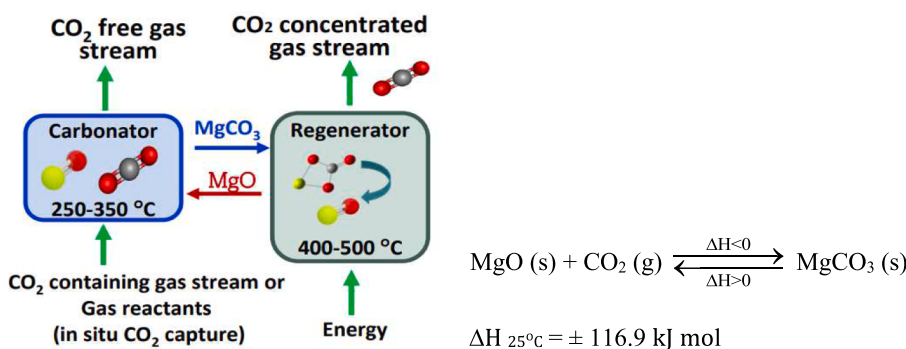


**Fig. 1.** Cyclic CO<sub>2</sub> removal process based on MgO sorbents.

has been investigated in both post and pre-combustion CO<sub>2</sub> capture technologies (Harada et al., 2015; Yang et al., 2018). For the case of pre-combustion conditions, the use of MgO sorbents in sorption enhanced water gas shift (SEWGS) reactions has gained relevance because it contributes to the increase of H<sub>2</sub> production and purity (Teixeira et al., 2022). Comparatively with other solid sorbents, MgO has a high theoretical capture capacity (1.09 g of CO<sub>2</sub>/g of MgO), affordable price, availability, and a medium regeneration temperature (~500 °C). Fig. 1 shows a diagram of the cyclic CO<sub>2</sub> removal process based on MgO sorbents.

The main drawback of using MgO as sorbent, is its poor sorption capacity coupled with slow kinetics and low thermal stability. The poor CO<sub>2</sub> sorption capacity may be due to the inactive bulk MgO, whereas the slow kinetics is mainly due to the formation of a monolayer of monodentate carbonate species at the MgO particles surface, which hinders the CO<sub>2</sub> diffusion. Several techniques were applied to enhance the CO<sub>2</sub> capture capacity: synthesis of nanosized MgO (Chammingkwan et al., 2021; Chang et al., 2022), dispersion of MgO on porous inert support (Han et al., 2012; Hanif et al., 2019), use of different precursors (Chen et al., 2019; Wang et al., 2020) and alkali molten salts (AMS) doping (Cui et al., 2020; Kwak et al., 2019). Hu (Hu et al., 2019) and Ruhimi (Ruhaimi et al., 2021) present an extensive review about the MgO sorbents progress, and summarize the main approaches described in literature to enhance the MgO based sorbents CO<sub>2</sub> capture capacity.

The use of CaCO<sub>3</sub> and CeO<sub>2</sub> as supports seems especially interesting due to the improved CO<sub>2</sub> capture capacity observed, namely 0.58 g CO<sub>2</sub>/g sorbent after 20 cycles (Cui et al., 2018a,b) and 0.43 g CO<sub>2</sub>/g sorbent after 30 cycles (Jin et al., 2019), respectively. Papalas (Papalas et al., 2021a) investigate the kinetics of carbonation of mixed oxides, using a low molar ratio of CaCO<sub>3</sub> to MgO (0.05/1), and conclude that the formation of MgCO<sub>3</sub> and CaMg(CO<sub>3</sub>)<sub>2</sub> occurs faster. Cui (Cui et al., 2020b) perform kinetic studies with CaO and MgO precursors and verify that the activation enthalpy of CO<sub>2</sub> sorption for AMS-Mg<sub>90</sub>Ca<sub>10</sub> is lower than for the case of AMS-MgO, indicating that the CaCO<sub>3</sub> decreases the activation energy of CO<sub>2</sub> sorption on MgO. Xiong (Xiong et al., 2021) observe that the Ce incorporation contributes to the formation of smaller MgO crystallites, increases the BET surface area and the availability of the alkaline sites. Consequently, the undoped MgO sorbents reach saturation faster than the doped sorbent. Besides, the CeO<sub>2</sub> increases the MgO sorbent basicity (Yu et al., 2018), which contributes to a better CO<sub>2</sub> sorption capacity of MgO sorbent.

The doping with alkali carbonates and the alkali nitrates/nitrites is the most widely recognized promising approach to enhance the CO<sub>2</sub> uptake (Gao et al., 2018; Chen et al., 2021). To the best of our knowledge, the first studies performed with molten salts were done by Zhang (Zhang et al., 2014). It was suggested that the NaNO<sub>3</sub> molten nitrate dissolves the bulk MgO, leading to [Mg<sup>2+</sup> ... O<sup>2-</sup>] ionic pairs, thus overcoming its high lattice energy barrier for carbonation. Harada (Harada et al., 2015) also showed that the carbonation of MgO coated

with a ternary mixture of Li, Na, and K nitrates performs faster. The authors suggest that during carbonation the molten layer of nitrates acts as a diffusion medium for CO<sub>2</sub>, improving the contact between MgO and the CO<sub>2</sub>, and controlling the unidentate carbonates formation.

However, there are still some doubts about the mechanisms associated with the MgO carbonation in presence of the alkali molten salts, i.e., the direct participation of the alkali metals in the reaction mechanism is still unclear, and contradictory results have been recently obtained using advanced characterization technologies (Landuyt et al., 2022; Gao et al., 2022). Gao (Gao et al., 2022) use *in situ* environmental transmission electron microscopy (eTEM) and CO<sub>2</sub> chemisorption by diffuse-reflectance infrared Fourier transform spectroscopy (DRIFTS) to understand the mechanism of the CO<sub>2</sub> interaction with the molten salt-MgO. The evolution of the molten NaNO<sub>3</sub> salt was tracked through the transient <sup>18</sup>O-isotopic exchange, and due the transfer of <sup>18</sup>O<sup>2-</sup> from the <sup>18</sup>O-nitrate to the MgO, it was stated that the molten salt participates actively in the MgCO<sub>3</sub> formation. Opposite results were achieved by Landuyt (Landuyt et al., 2022), by using Raman spectroscopy and *in situ* thermogravimetric analysis in combination with mass spectrometry to track the <sup>18</sup>O label in the MgCO<sub>3</sub>, NaNO<sub>3</sub>, and CO<sub>2</sub> phases during carbonation and decarbonation reactions. It was observed a rapid oxygen exchange between CO<sub>2</sub> and MgO through the reversible formation of surface carbonates, and no oxygen exchange was observed between NaNO<sub>3</sub> and CO<sub>2</sub> or NaNO<sub>3</sub> and MgO.

The melting temperature and the wetting properties can also influence the CO<sub>2</sub> uptake. Dal Pozzo (Dal Pozzo et al., 2019) investigate the melting point of several nitrates and their mixtures and achieve melting temperatures between 120 °C for a mixture with 18/30/52 of LiNO<sub>3</sub>/NaNO<sub>3</sub>/KNO<sub>3</sub>, 255 °C for LiNO<sub>3</sub>, 308 °C for NaNO<sub>3</sub> and 334 °C for KNO<sub>3</sub>. The lower melting temperature of the eutectic LiNO<sub>3</sub>/NaNO<sub>3</sub>/KNO<sub>3</sub> mixture facilitates the fast dissolution of CO<sub>2</sub>, increasing the carbonate ions supersaturation, and MgCO<sub>3</sub> nucleation and growth.

Jo (Jo et al., 2017) verify that the MgO and the MgCO<sub>3</sub> in contact with the NaNO<sub>3</sub> have different wetting properties because the former has a more ionic bonding character, allowing an enhanced distribution of NaNO<sub>3</sub> on the MgO surface, that can be lost after the MgCO<sub>3</sub> formation, justifying the sorbents deactivation along the cycles.

In this work the CO<sub>2</sub> uptake and cyclic stability of MgO sorbents unsupported and supported with CaCO<sub>3</sub> and CeO<sub>2</sub>, both doped with an alkali molten salts mixture (15 % of NaNO<sub>3</sub>, LiNO<sub>3</sub> and KNO<sub>3</sub> (18/30/52), is evaluated along 10 carbonation-calcination cycles. The experiments were carried out in a fixed-bed reactor under two different carbonation atmospheres, namely, 100 % of CO<sub>2</sub> and 25 % of CO<sub>2</sub> balanced in air. The effect of the CaCO<sub>3</sub> and CeO<sub>2</sub> supports on the stability of the MgO sorbents and on the AMS distribution along the MgO surface, is illustrated on a scheme, that was validated experimentally. SEM, N<sub>2</sub> sorption and XRD techniques performed with the sorbent before and after the AMS activation at 450 °C, and after 10 carbonation-calcination cycles, demonstrate the changes on MgO sorbents.

**Table 1**

Summary of the molar composition of unsupported and supported MgO sorbents.

Magnesium (mol, %)	Support (mol, %)	Sample ID
100	0	MgO-SG
90	10 Ce	MgO-Ca-SG
90	10 Ca	MgO-Ce-SG

## 2. Experimental section

### 2.1. Synthesis of unsupported and supported MgO based sorbents

The unsupported sorbents were prepared with magnesium nitrate hexahydrate ( $\text{Mg}(\text{NO}_3)_2 \cdot 6\text{H}_2\text{O}$ ) from Sigma-Aldrich (assay of 98 – 102 %) and citric acid monohydrate ( $\text{C}_6\text{H}_8\text{O}_7 \cdot \text{H}_2\text{O}$ ) from Panreac (assay of 99.5 – 102 %). As performed in a previous work, both were dissolved in distilled water, with a molar ratio of citric acid and distilled water to magnesium of 1:1 and 120:1, respectively (Teixeira et al., 2019). Relatively to supported MgO sorbents, the same procedure was used, but two different types of supports were added: calcium nitrate tetrahydrate ( $\text{Ca}(\text{NO}_3)_2 \cdot 4\text{H}_2\text{O}$ ) or cerium nitrate hexahydrate ( $\text{Ce}(\text{NO}_3)_3 \cdot 6\text{H}_2\text{O}$ ), both from Sigma-Aldrich (assay  $\geq 99\%$ ). Each solution was continuously stirred in a silicone oil bath at 80 °C for 6 h. Subsequently, the wet gel was dried in the oven at 120 °C for 14 h. After drying, the resultant sample was calcined in the muffle by ramping the temperature to 500 °C at a rate of 2 °C/min plus 2 h more at 500 °C. Table 1 summarizes the all-prepared samples of unsupported and supported MgO-based sorbents, and respective identification. The support molar fraction was defined based on literature (Jin et al., 2019a; Papalas et al., 2021b).

The ternary alkali metal salts (AMS) doping was performed with a mixture of 18 mol% of  $\text{NaNO}_3$ , 30 mol% of  $\text{LiNO}_3$  and 52 mol % of  $\text{KNO}_3$ . The used AMS reagents are from Sigma-Aldrich (assay  $\geq 99\%$ ). The synthesized unsupported and supported samples of MgO sorbents were doped using the wet impregnation method. The wet-impregnation followed procedure consisted of the dissolution of both MgO-based sorbent and AMS in 20 ml of distilled water, using magnetic stir for 1 h at room temperature. The obtained aqueous slurry was dried in the oven at 120 °C for 14 h. Subsequently, the dried sample was placed in the muffle for calcination using a heating rate of 2 °C/min until it reached 450 °C plus 4 h at 450 °C. The following nomenclature was used for the doped sorbent samples: x(Na-Li-K)-MgO, where x corresponds to the molar fraction (%) of AMS; or x(Na-Li-K)-MgO-Y, where Y corresponds to the Ca or Ce support.

## 2.2. Characterization methods

The textural properties of fresh and used sorbents were assessed by  $\text{N}_2$  sorption technique at –196 °C (Quantachrome Instruments, Model autosorb IQ). The degasification procedure was performed in two steps: the first one at 90 °C for 1 h and the second one at 350 °C for 5 h. The ASiQwin software from Quantachrome was used to collect and analyze the sorbent's specific area ( $S_{\text{BET}}$ ) using the BET method; the pore size distribution (PSD) using BJH model (desorption branch); and the total pore volume ( $V_p$ ) at a relative pressure ( $p/p_0$ ) of 0.95. The mineralogical characterization of the sorbents was investigated using X-ray powder diffraction (XRD) in the Bruker D8 Advance diffractometer set up with a 1D detector (SSD 160), a  $\text{Cu K}\alpha$  ( $\lambda = 0.15406\text{ nm}$ ) and a Ni filter. Each sample was scanned within the 2θ range of 5–80 °, with a step size of 0.03° and a step time of 0.5 s. The crystallography open database (COD) was used to identify the crystalline phases and the Scherrer's ( $D = K\lambda/b\cos\Theta$ ) equation to determine the  $\text{CaO}$  crystallite size. For comparative reasons a commercial MgO (Sigma-Aldrich) was also characterized. The morphology of fresh and spent sorbents, that is, before and after the experiments carried out in a fixed-bed reactor, was investigated via scanning electron microscopy (SEM) performed in a Phenom Pro G6 from Thermo Scientific.

### 2.3. Fixed bed reactor $\text{CO}_2$ uptake studies

The  $\text{CO}_2$  uptake studies were performed in a fixed bed reactor consisting of 10 carbonation-calcination cycles with carbonation (~30 min) and complete calcination (6 to 15 min), at 280 °C and 400 °C, respectively. The sorbent (~0.75 g) was loaded to the surface of the porous plate of the quartz reactor (14 cm of high and 5 cm of internal diameter), and pre-activated at 400 °C under air atmosphere (10 °C/min). The packing densities were c.a. 0.4  $\text{g/cm}^3$ , 0.3  $\text{g/cm}^3$  and 0.1  $\text{g/cm}^3$  for 15(Na,K,Li)-MgO, 15(Na,K,Li)-MgO-Ca and 15(Na,K,Li)-MgO-Ce, respectively. Since the sorbent mass was maintained constant, the packing length was between c.a. 1 and 3.5 mm. After the calcination step, the reactor temperature was cooled down to 280 °C and the carbonation step was performed with 100 % of  $\text{CO}_2$  or 25 % of  $\text{CO}_2$  balanced in air, followed in both cases by the calcination under 100 % of air. The inlet gas flow (1000 ml/min) was controlled with Alicat and Brooks mass flowmeters for air and  $\text{CO}_2$  flows, respectively, while the  $\text{CO}_2$  gas concentration at the outlet stream during the carbonation-calcination cycles was measured with a Guardian NG equipment whose range of measurement is 0–30 % (accuracy: 2 % of full scale). An Eurotherm® 2000 series equipment controlled the oven temperature and a type K thermocouple monitored the temperature inside the reactor. A Labview software interface was used for data acquisition.

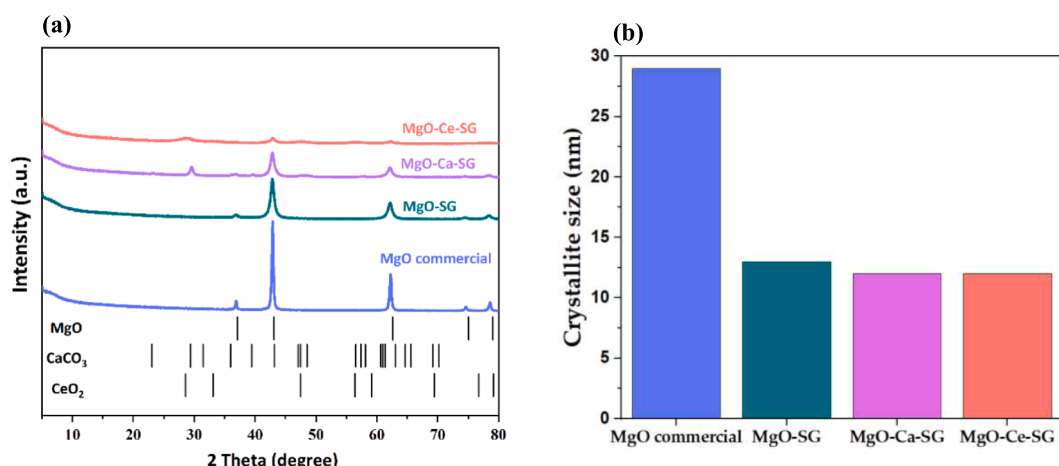
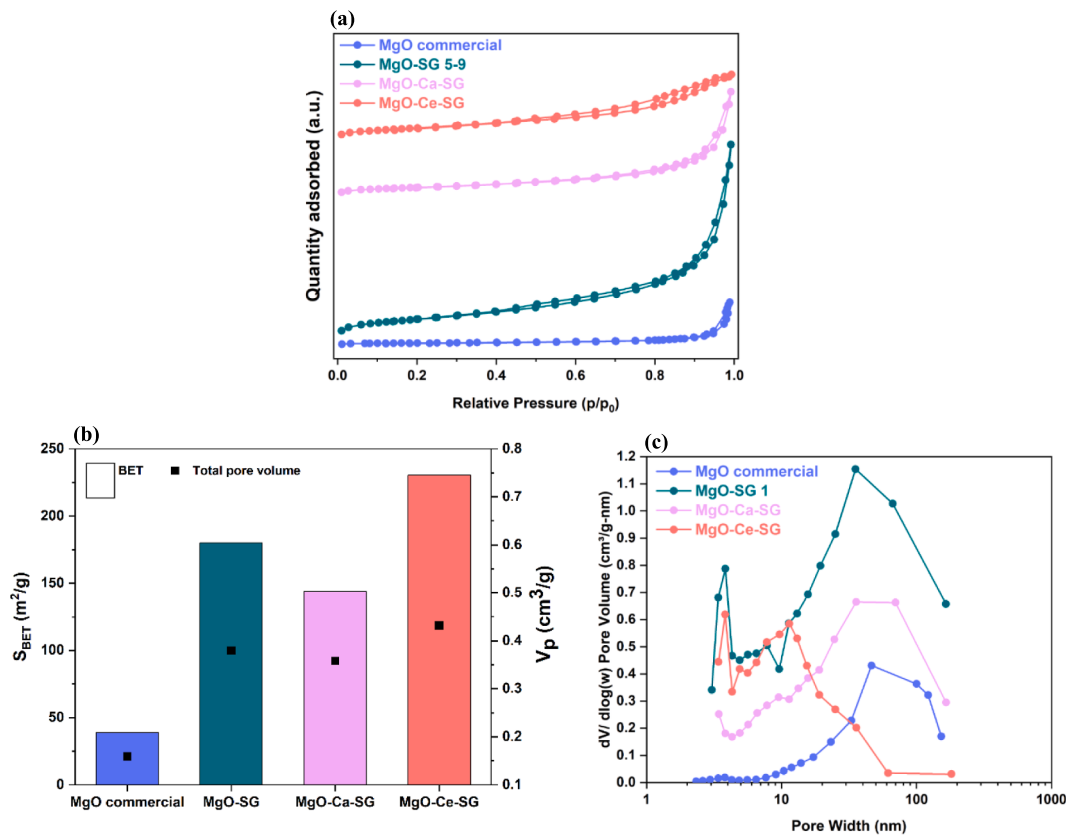


Fig. 2. Unsupported (MgO-SG), supported (MgO-Ca-SG and MgO-Ce-SG) and commercial MgO properties: (a) XRD patterns, (b) MgO crystallite size.



**Fig. 3.** Unsupported (MgO-SG), supported (MgO-Ca-SG and MgO-Ce-SG) and commercial MgO properties: (a) N<sub>2</sub> isotherms, (b) Specific Surface Area (S<sub>BET</sub>) and total pore volume (V<sub>p</sub>) and (c) Pore size distribution (PSD) estimated by the BJH desorption.

After the carbonation step, carried out with 25 % or 100 % of CO<sub>2</sub>, the captured CO<sub>2</sub> was released and quantified using a calcination atmosphere with 100 % of air. The molar amount of the CO<sub>2</sub> released during the calcination, n<sub>CO<sub>2</sub>, calcination</sub>, was determined with the following Eq. (1):

$$n_{CO_2, \text{calcination}} = \int_{t_1}^{t_2} (n_{CO_2, \text{captured}}) dt \quad (1)$$

Where n<sub>CO<sub>2</sub>, captured</sub> is the molar amount of CO<sub>2</sub> released by the sorbent between the start and end times of the calcination reaction t<sub>1</sub> and t<sub>2</sub>, respectively.

The MgO conversion (%) of the sorbent, i.e., conversion of MgO to MgCO<sub>3</sub> during the carbonation step, was obtained using the following Eq. (2):

$$\text{MgO}_{\text{conversion}} = \frac{n_{CO_2, \text{calcination}} \times M_{MgO}}{m_{\text{sorbent}} \times w_{MgO-\text{sorbent}}} \times 100 (\%) \quad (2)$$

Where n<sub>CO<sub>2</sub>, calcination</sub> represents the molar amount of CO<sub>2</sub> (mol) captured and released during the calcination step; M<sub>MgO</sub> represents the molar mass of MgO (g/mol), m<sub>sorbent</sub> represents the mass of sorbent (g); and w<sub>MgO-sorbent</sub> represents the nominal mass fraction of the MgO (% wt.) in the sorbent.

### 3. Results and discussion

#### 3.1. Properties of unsupported and supported MgO-based sorbents

The x-ray diffraction peaks and the MgO crystallite size assessed for all the unsupported and supported sorbents, as well as for the commercial MgO is illustrated on the Fig. 2(a) and (b), respectively.

Fig. 2(a) shows that all the XRD patterns of the synthesized sorbents exhibit the characteristic peaks of the MgO pattern [42.9° (2, 0, 0), 62.2°

(2, 2, 0), 78.5° (2, 2, 2)], as expected. This evidence indicates that both the synthesis by sol-gel method and the calcination pre-treatment at 500 °C were well succeeded. In addition, XRD patterns of the supported MgO-Ca-SG and MgO-Ce-SG sorbents also present the characteristic peaks of the correspondent XRD pattern support at 29.4° (-1, 1, 4) and at 28.5° (-1, -1, -1), for CaCO<sub>3</sub> and CeO<sub>2</sub>, respectively, suggesting that the addition of support was successful. The MgO-SG, MgO-Ca-SG and MgO-Ce-SG sorbents registered a crystallite size between 12 and 13 nm, respectively, against that of the commercial MgO of 28 nm [Fig. 2(b)]. Thus, the use of the sol-gel method to synthesize MgO sorbents was advantageous, since it allowed to obtain MgO sorbents with lower crystallite size that, in turn, should be directly correlated with higher surface areas, enhancing the CO<sub>2</sub> sorption (Wang et al., 2018). The size of MgO crystallites described in literature can vary a lot, and it can be correlated with the synthetization method. Thus, average crystallites size of 7–8 nm of a MgO sorbent can be obtained through the calcination of pure hydromagnesite (HM) (Dal Pozzo et al., 2019), but values around to 100 nm are also described, for example, when sol-gel method is applied using different gelling agents and calcination temperatures (Jeevanandam et al., 2019).

The N<sub>2</sub> sorption-desorption isotherms of the MgO-SG and MgO-Ce-SG sorbents shown in [Fig. 3(a)] can be considered between type II and IV, accordingly to IUPAC's classification (Thommes et al., 2015). The hysteresis loop of the MgO-Ce-SG sorbent is classified as type H4, which is typical of mesoporous materials. The hysteresis loop of the MgO-SG is classified as type H3 that is often associated with macroporous materials. The N<sub>2</sub> sorption-desorption isotherms of the commercial MgO and MgO-Ca-SG are classified as type II, that are features of macroporous materials. The S<sub>BET</sub> results demonstrated to be in line with the XRD characterization. The synthesized sorbents MgO-SG, MgO-Ca-SG and MgO-Ce-SG exhibited a S<sub>BET</sub> of 180 m<sup>2</sup>/g, 144 m<sup>2</sup>/g and 230 m<sup>2</sup>/g, respectively, that is higher than that of the commercial MgO of 39 m<sup>2</sup>/

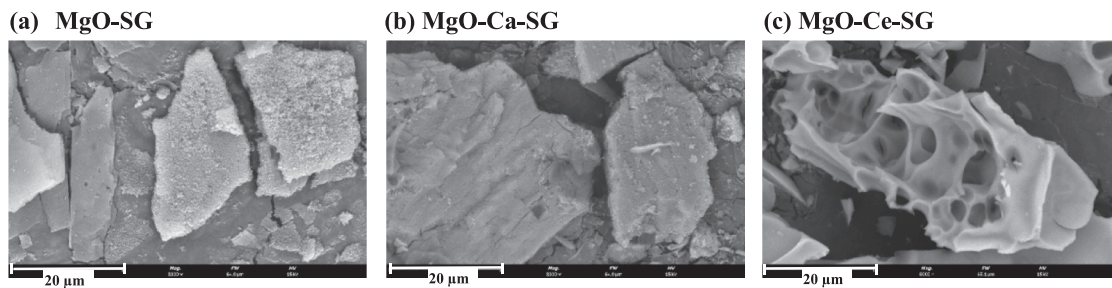


Fig. 4. SEM images of (a) MgO-SG, (b) MgO-Ca-SG and (c) MgO-Ce-SG (scale: 20  $\mu\text{m}$  and magnification:  $\times 8000$ ).

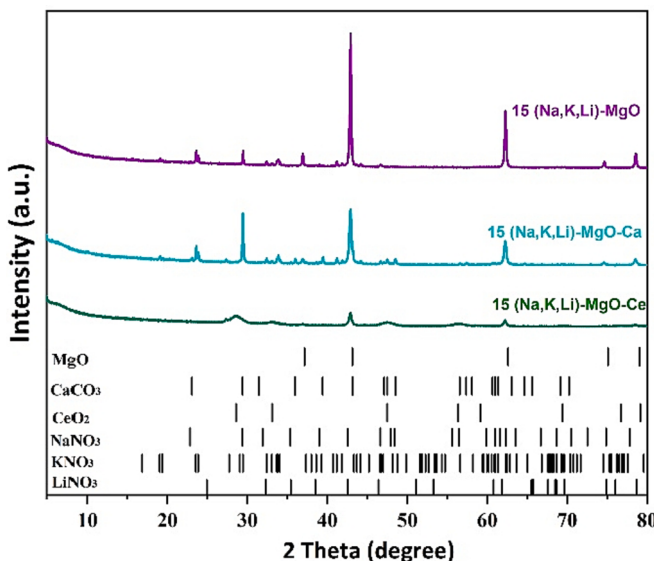


Fig. 5. XRD patterns of sorbents doped with  $\text{NaNO}_3$ ,  $\text{LiNO}_3$  and  $\text{KNO}_3$ : 15 (Na, K, Li)-MgO, 15 (Na, K, Li)-MgO-Ca and 15 (Na, K, Li)-MgO-Ce.

g [Fig. 3(b)]. So, it was confirmed that smaller MgO crystallite's size did correspond to higher sorbents' surface areas. Moreover, the synthesized sorbents exhibit higher total pore volume than the MgO commercial, which is expected to facilitate the  $\text{CO}_2$  sorption process, as the resistance through diffusion decreases inside of the pores as its volume expands (Hu et al., 2019b). In addition, the PSD of the MgO-Ce-SG sorbent [Fig. 3(c)] indicates a constitution of mainly mesoporous ( $2 - 50 \text{ nm}$ ), which is in line with the evidence provided by the correspondent  $\text{N}_2$  isotherms' characterizations. There is also a small percentage of macroporous ( $> 50 \text{ nm}$ ). Both the commercial MgO and MgO-SG-Ca consist of macroporous predominantly, although the MgO-SG-Ca also exhibits a small share of mesoporous. The PSD of the MgO-SG sorbent reveals the existence of both meso and macroporous.

As mentioned above, the properties of synthesized MgO found in literature using sol-gel method vary considerably.  $S_{\text{BET}}$  values of  $66 \text{ m}^2/\text{g}$  (Duong et al., 2019) and  $191 \text{ m}^2/\text{g}$  (Salman et al., 2021) can be found, which are in agreement with the present study. By aerogel method, the  $S_{\text{BET}}$  can reach  $569 \text{ m}^2/\text{g}$  (Vu et al., 2014), but it will also increase the manufacturing costs, as it uses a high-pressure autoclave and organics during the synthesis, that, in turn, also impacts negatively the environment. The synthesized MgO-Ca-SG presents higher  $S_{\text{BET}}$  ( $144 \text{ m}^2/\text{g}$ ) and lower crystallite size (12 nm) than the MgO-10Ca reported by Jin et al., namely,  $35 \text{ m}^2/\text{g}$  and 21 nm (Jin et al., 2018). The synthesized MgO-Ce-SG presents similar  $S_{\text{BET}}$  ( $230 \text{ m}^2/\text{g}$ ) than the MgO-10Ce described by Jin et al., namely,  $252 \text{ m}^2/\text{g}$  (Jin et al., 2019).

The comparison of SEM images [Fig. 4(a)] with [Fig. 4(b)] indicates that the addition of support did not change the overall sheet-like

Table 2

Crystallite size of unsupported (MgO-SG) and supported sorbents (MgO-Ca-SG and MgO-Ce-SG) before and after doping with 15% of ternary mixture of (Na, Li, K) $\text{NO}_3$ .

Crystallite size (nm)	MgO-SG	MgO-Ca-SG	MgO-Ce-SG
0 % (Na, Li, K) $\text{NO}_3$	13	12	12
15 % (Na, Li, K) $\text{NO}_3$	26	30	27

morphology of the MgO sorbent, that appeared to maintain a compact and smooth surface after the addition of the Ca support. Conversely, the differences are notable from SEM images [Fig. 4(a)] to [Fig. 4(c)]. The addition of a Ce support provoked the formation of an internal structure consisting of numerous spherical empty holes of different diameters, in accordance with the mesoporous nature of the MgO-SG-Ce sorbent concluded from the  $\text{N}_2$  sorption characterization.

### 3.2. Properties of MgO-based sorbents doped with AMS

The unsupported (MgO-SG) and supported sorbents (MgO-Ca-SG and MgO-Ce-SG) were doped with 15 % of a ternary mixture of (Na, Li, K) $\text{NO}_3$ . Fig. 5 shows the x-ray diffraction peaks of the 15 (Na, K, Li)-MgO, 15 (Na, K, Li)-MgO-Ca and 15 (Na, K, Li)-MgO-Ce sorbents after the AMS doping. Table 2 summarizes the MgO crystallite size of sorbents after the AMS doping.

The XRD patterns of the impregnated sorbents maintains the characteristic peaks of the MgO pattern [ $42.9^\circ$  ( $2, 0, 0$ ),  $62.2^\circ$  ( $2, 2, 0$ ),  $78.5^\circ$  ( $2, 2, 2$ )], as well as the main peaks of the XRD pattern of  $\text{CaCO}_3$  [ $29.4^\circ$  ( $-1, 1, 4$ )] and of the  $\text{CeO}_2$  [ $28.5^\circ$  ( $-1, -1, -1$ )] for 15 (Na, Li, K)-MgO-Ca and 15 (Na, Li, K)-MgO-Ce, respectively. Regarding to the nitrate salts used in the impregnation,  $\text{LiNO}_3$  was not detected by XRD in any of the patterns of the analyzed sorbents, as expected. In fact, it is stated in literature that lithium has a small crystallite size and, thus, a good dispersion in the sorbent (Papalas et al., 2021a). The main peaks of the  $\text{KNO}_3$  pattern [ $23.5^\circ$  ( $-1, -1, 1$ ) and  $29.4^\circ$  ( $0, -1, -2$ )] were identified in the XRD patterns of the 15 (Na, Li, K)-MgO and in the 15 (Na, Li, K)-MgO-Ca, as well as the main peaks of the  $\text{NaNO}_3$  pattern [ $29.4^\circ$  ( $-1, 1, 4$ ),  $38.9^\circ$  ( $-2, 1, -3$ ),  $47.9^\circ$  ( $-1, 1, 8$ )]. The characteristic peak of the  $\text{CeO}_2$  XRD pattern is very wide, so it makes impossible to identify the peak at  $29.4^\circ$  of the  $\text{KNO}_3$  and  $\text{NaNO}_3$  patterns. Table 2 shows that the AMS doping affected the crystallite size of the unsupported and supported sorbents, leading to its increase.

The  $\text{N}_2$  sorption-desorption isotherms [Fig. 6(a)] of 15 (Na, Li, K)-MgO, 15 (Na, Li, K)-MgO-Ca and 15 (Na, Li, K)-MgO-Ce sorbents are more similar to type II, characteristic of macroporous materials. As expected, the AMS doping seems to have affected MgO-SG and the MgO-Ce-SG, both prior classified as between type II and IV isotherms, for presenting a more pronounced hysteresis as fresh sorbents.

The 15 (Na, Li, K)-MgO sorbent presents the highest  $S_{\text{BET}}$  ( $32 \text{ m}^2/\text{g}$ ) that is very similar to that of the 15 (Na, Li, K)-MgO-Ce ( $31 \text{ m}^2/\text{g}$ ). The 15 (Na, Li, K)-MgO-Ca exhibits the smallest  $S_{\text{BET}}$  ( $18 \text{ m}^2/\text{g}$ ). Moreover, all the sorbents analyzed in this set verified a reduction in their  $S_{\text{BET}}$  with

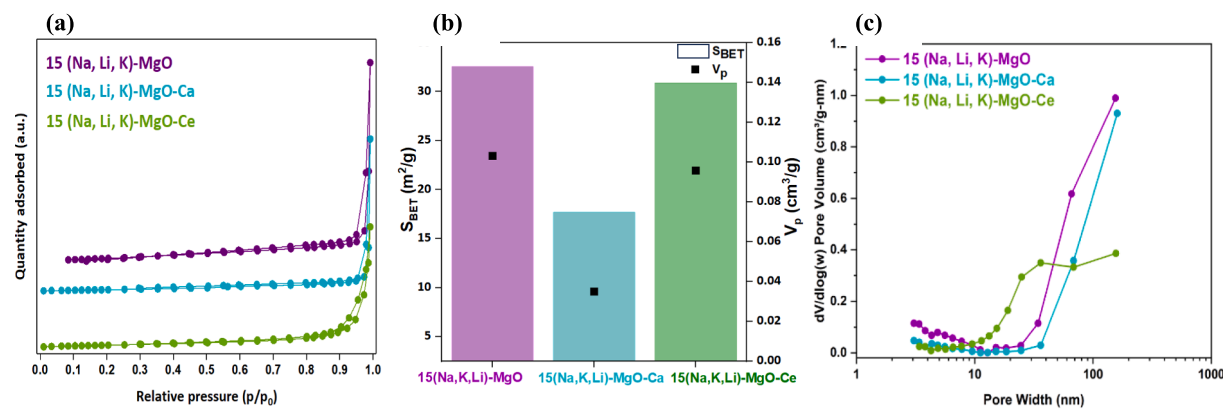


**Fig. 6.** MgO-SG, MgO-Ca-SG and MgO-Ce-SG after impregnation with 15 % of (Na, Li, K)NO<sub>3</sub>: (a) N<sub>2</sub> isotherms, (b) Specific Surface Area ( $S_{BET}$ ) and total pore volume ( $V_p$ ) and (c) Pore size distribution (PSD) estimated by the BJH desorption.

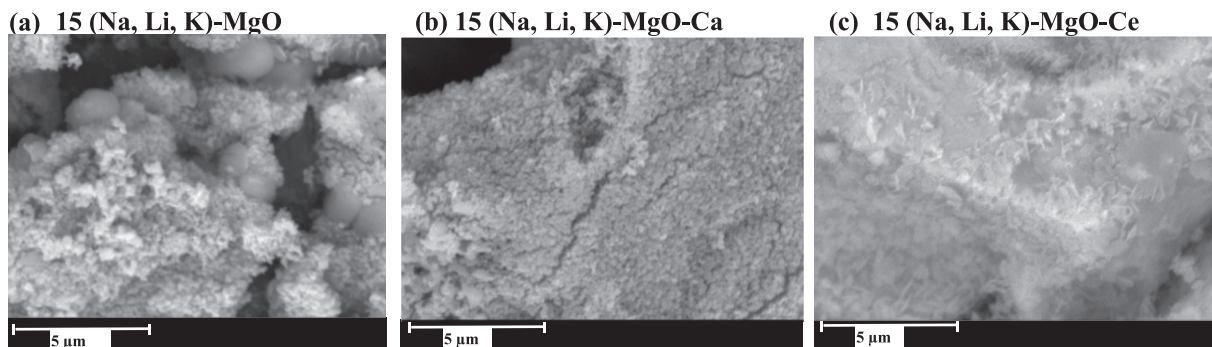


**Fig. 7.** SEM images of (a) 15 (Na, Li, K)-MgO, (b) 15 (Na, Li, K)-MgO-Ca and (c) 15 (Na, Li, K)-MgO-Ce sorbents (scale: 5  $\mu$ m and magnification: x 30 000).

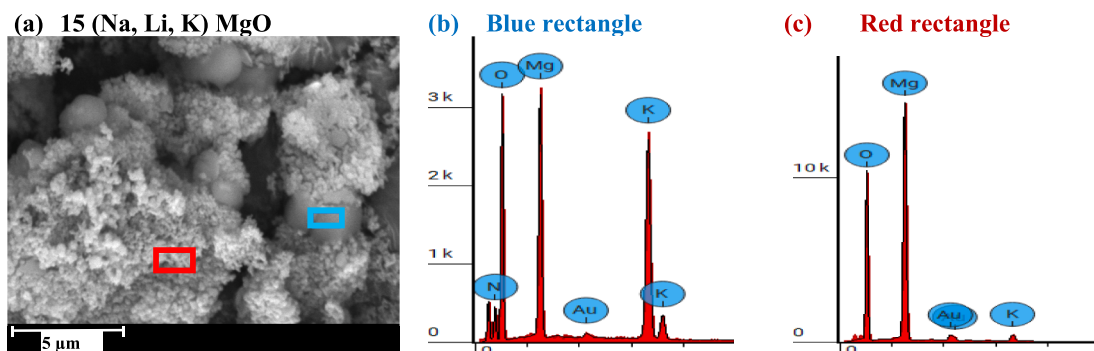


**Fig. 8.** SEM image of (a) 15 (Na, Li, K) MgO sorbent, and identification of main elements acquired by energy dispersive x-ray spectrometer (qualitative analysis): (b) blue rectangle and (c) red rectangle.

respect to before the impregnation (Fig. 3). This evidence is in line with the previous conclusions from the XRD characterization, in which it was detected an increase of the MgO crystallite size, indicating a reduced surface area available for the MgO sorbent to uptake CO<sub>2</sub>. Dal Pozzo et al. reported a  $S_{BET}$  of 22  $m^2/g$  for a MgO sorbent promoted with 10 % of (Na, Li, K) NO<sub>3</sub> (Dal Pozzo et al., 2019), which is smaller than that of 15 (Na, Li, K)-MgO and 15 (Na, Li, K)-MgO-Ce sorbents, but higher than that of 15 (Na, Li, K)-MgO-Ca. In addition, all the analyzed sorbents of the set also registered a decreased of the total pore volume after AMS doping, due to its partial occupation by the ternary alkali mixture (Park et al., 2020), which should affect the CO<sub>2</sub> sorption due to the higher occurrence of pores' blocking. The PSD of the 15 (Na, Li, K)-MgO, 15 (Na, Li, K)-MgO-Ca and 15 (Na, Li, K)-MgO-Ce sorbents indicates a constitution of mainly macropores (>50 nm), as expected according to

the detected AMS impact on the type of isotherms. A small share of mesoporous is also present though, especially in the case of 15 (Na, Li, K)-MgO-Ce.

Fig. 7 shows the SEM images of 15 (Na, Li, K)-MgO, 15 (Na, Li, K)-MgO-Ca and 15 (Na, Li, K)-MgO-Ce sorbents and Fig. 8 shows the identification of the main elements present in specific zones of 15 (Na, Li, K)-MgO, acquired by energy dispersive x-ray spectrometer (EDS).

The SEM images of the unsupported 15 (Na, Li, K)-MgO sorbent reveal the presence of several "spherical" structures with smooth surface that are not present in the SEM images of both the supported 15 (Na, Li, K)-MgO-Ca and 15 (Na, Li, K)-MgO-Ce sorbents. These structures are associated with the sintering phenomenon that results from the melting of some species (further identified by EDS). Thus, evidence suggests that the addition of supports to MgO-based sorbents prevents the sintering to

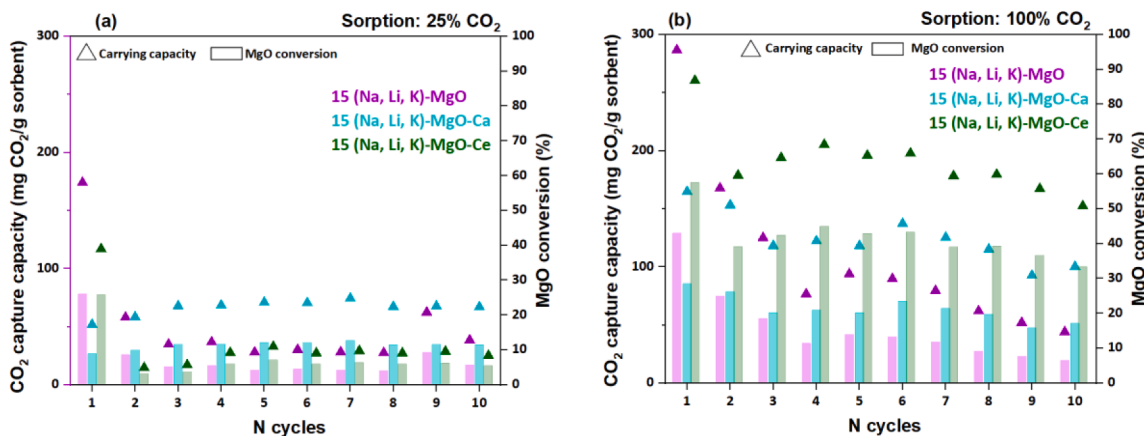


**Fig. 9.** Capture capacity (mg CO<sub>2</sub>/g sorbent) and MgO conversion (%) achieved along 10 carbonation- calcination cycles in a fixed bed unit carried out with 15 (Na, Li, K)-MgO, 15 (Na, Li, K)-MgO-Ca and 15 (Na, Li, K)-MgO-Ce sorbents using the following conditions: (a) carbonation with 100 % CO<sub>2</sub> at 280 °C and calcination with 100 % air at 400 °C, (b) carbonation with 25 % CO<sub>2</sub> at 280 °C and calcination with 100 % air at 400 °C.

occur and, in turn, the agglomeration of MgO particles by melting (Vu et al., 2014). Instead, it provides the well dispersion of it, which should improve the CO<sub>2</sub> sorption process. In addition, the surface of the 15 (Na, Li, K)-MgO-Ce sorbent exhibits some crystal structures, which seem haphazardly overlapping sheets. Fig. 8 shows the comparison of the EDS obtained for a sintered (blue rectangle) and for a non-sintered zone (red rectangle) of 15 (Na, Li, K) MgO sorbent. The sintered zone is mainly constituted by K instead of Mg, conversely to what is verified for the non-sintered zone's constitution. Hence, EDS indicates that the sintering of the unsupported MgO sorbent corresponds to the melting of KNO<sub>3</sub>. In fact, the melting point of KNO<sub>3</sub>, that is 334 °C (Vu et al., 2014) was surpassed by the calcination pre-treatment temperature of 450 °C.

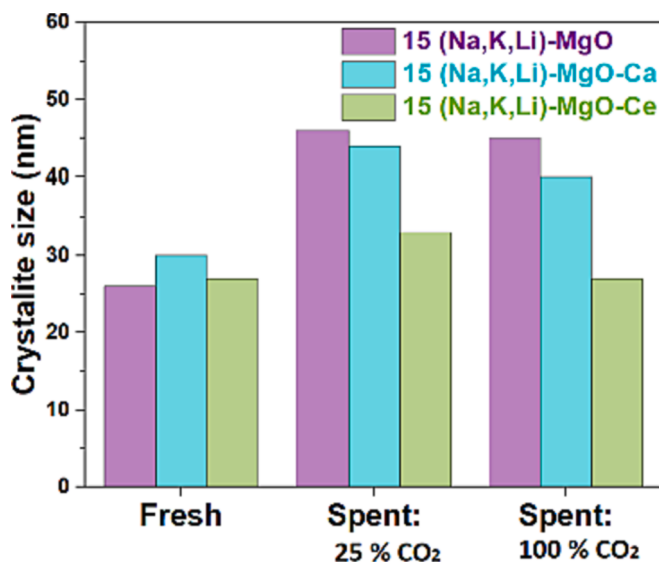
### 3.3. CO<sub>2</sub> carbonation-calcination cycles in a fixed bed reactor

Fig. 9 (a) and Fig. 9(b) plot the capture capacity and the MgO conversion of the 15 (Na, Li, K)-MgO, 15 (Na, Li, K)-MgO-Ca and 15 (Na, Li, K)-MgO-Ce sorbents over the 10 cyclic CO<sub>2</sub> carbonation- calcination tests conducted in the fixed-bed reactor under carbonation atmospheres of 100 % of CO<sub>2</sub> and 25 % of CO<sub>2</sub>, respectively.

A general comparison of Fig. 9(a) and Fig. 9(b) shows higher values of capture capacity and percentages of MgO conversion under a carbonation atmosphere of 100 % CO<sub>2</sub> for both sets of sorbents, as expected. CO<sub>2</sub> concentration functions as a driving force for the diffusion and sorption of CO<sub>2</sub> molecules at the carbonation step, so higher CO<sub>2</sub> concentrations means higher contact between the sorbent and CO<sub>2</sub> (Hu et al., 2019b). Focusing on Fig. 9(a), unsupported MgO sorbent performed worse than any of the supported MgO sorbents, concerning to CO<sub>2</sub> uptake, thus, it presents the lowest MgO conversion values of the set as the number of cycles increases, although it registered a higher MgO conversion at the 1st cycle than the 15 (Na, Li, K)-MgO-Ca sorbent. This behaviour was expected, and it is the result of the non-addition of support, that as mentioned above increase the availability of well-exposed basic active sites, helping on the carbonation reaction. It started with an abrupt decreasing tendency from the 1st to the 4th cycle, with a small regain at the 5th cycle that is followed by a gradual decreasing of the MgO conversion until the 10th cycle. The Ca supported exhibits regains at the 4th, 6th and 10th cycles, showing higher values of MgO conversion than those of the unsupported sorbent. It was the Ce based supported sorbent that demonstrated to have the highest values of MgO conversion under 100 % of CO<sub>2</sub> carbonation atmosphere. About stability, both supported sorbents presented similar values of deactivation, i. e., 40 % and 42 % for 15 (Na, Li, K)-MgO-Ca and 15 (Na, Li, K)-MgO-Ce, respectively, while the unsupported sorbent deactivation was 85 %. Under an atmosphere consisting of 25 % of CO<sub>2</sub> balanced in air [Fig. 9

(b)], it was the Ca-based supported sorbent that presented the highest MgO conversion values. Moreover, it was the only sorbent that managed to increase its CO<sub>2</sub> uptake during the test, which can be due to the formation of the CaCO<sub>3</sub> during the first cycles, that can contribute to the sorbent stabilization, contributing for the CO<sub>2</sub> uptake. Therefore, between the 1st and 10th cycle the MgO conversion of 15 (Na, Li, K)-MgO-Ca increased 28 %, while the 15 (Na, Li, K)-MgO and 15 (Na, Li, K)-MgO-Ce sorbents deactivation was 78 % and 79 %, respectively. Hence, the 15 (Na, Li, K)-MgO-Ca was considered the sorbent best performing under a sorption atmosphere of 25 % of CO<sub>2</sub>, which make it the most promising sorbent under realistic industrial applications, where concentrations of CO<sub>2</sub> lower than 25 % in flue gases are often. The desorption curves of 15 (Na, K, Li)-MgO, 15(Na, K, Li)-MgO-Ca and 15(Na, K, Li)-MgO-Ce, for the 1st and 10th cycle carried out under 100 % of CO<sub>2</sub> or 25 % of CO<sub>2</sub> (balanced in air) atmosphere are shown in the [supplementary information](#) (S1). The CO<sub>2</sub> released during the calcination of all sorbents decreases between the 1st and 10th cycles and when a lower CO<sub>2</sub> driving force is used, i.e., 25 % vs. 100 % of CO<sub>2</sub>. Relatively to the inert support addition, the results show the high stability of the 15(Na, K, Li)-MgO-Ca since an abrupt desorption peak is observed with both atmospheres after 10 cycles, showing that the 15(Na, K, Li)-MgO-Ca sorbent is less influenced by the CO<sub>2</sub> molar fraction on the feed flue gas. For the 15(Na, K, Li)-MgO-Ce sorbent, the stability of the CO<sub>2</sub> capture capacity is evidenced for the experiments carried out with 100 % of CO<sub>2</sub>. The basicity of CeO<sub>2</sub> (Z. Cui et al., 2018) enhances its affinity with the CO<sub>2</sub> molecule as described by Yoshikawa (Yoshikawa et al., 2017), which can justify the improved performance of the sorbent under a higher CO<sub>2</sub> driving force, since more CO<sub>2</sub> is available to react with MgO and CeO<sub>2</sub>, reducing the negative effect of a possible competition between both oxides by CO<sub>2</sub>. A FTIR-operando technique should be used in future studies to confirm this hypothesis.

The comparison with literature is difficult since most of the times the experimental conditions are not the same, and most of the studies are performed in TGA equipment. For example, literature reports an MgO sorbent impregnated with (Li, K)NO<sub>3</sub> + (Na<sub>2</sub>K<sub>2</sub>)CO<sub>3</sub> that registered values of capture capacity of 410 mg CO<sub>2</sub>/g sorbent in 1st carbonation, while in the present study, for the 15 (Na, Li, K)-MgO sorbent it was between 174 and 287 mg CO<sub>2</sub>/g, for an atmosphere with 25 or 100 % of CO<sub>2</sub>, respectively. Yet it must consider that test was conducted under different carbonation and calcination conditions and in a packed bed reactor (Chen et al., 2021). Moreover, it is described in literature that packed bed reactors may be able to overcome limitations associated to fixed-bed configuration, namely, elevated pressure drops, gradients of temperature and both mass and heat transfers' limitation problems. In fact, conventional fixed-bed reactors are believed not to deliver the full



**Fig. 10.** MgO crystallite size of fresh and spent sorbents after 10 carbonation-calcination cycles performed under 25 % or 100 % of CO<sub>2</sub> carbonation atmosphere: 15 (Na, Li, K)-MgO, 15 (Na, Li, K)-MgO-Ca and 15 (Na, Li, K)-MgO-Ce.

potential associated to CO<sub>2</sub> uptake technologies. Conversely, packed configuration can be able to reduce the pressure drop by keeping an elevated contacting area between the gas and the solid (Dhole et al., 2021).

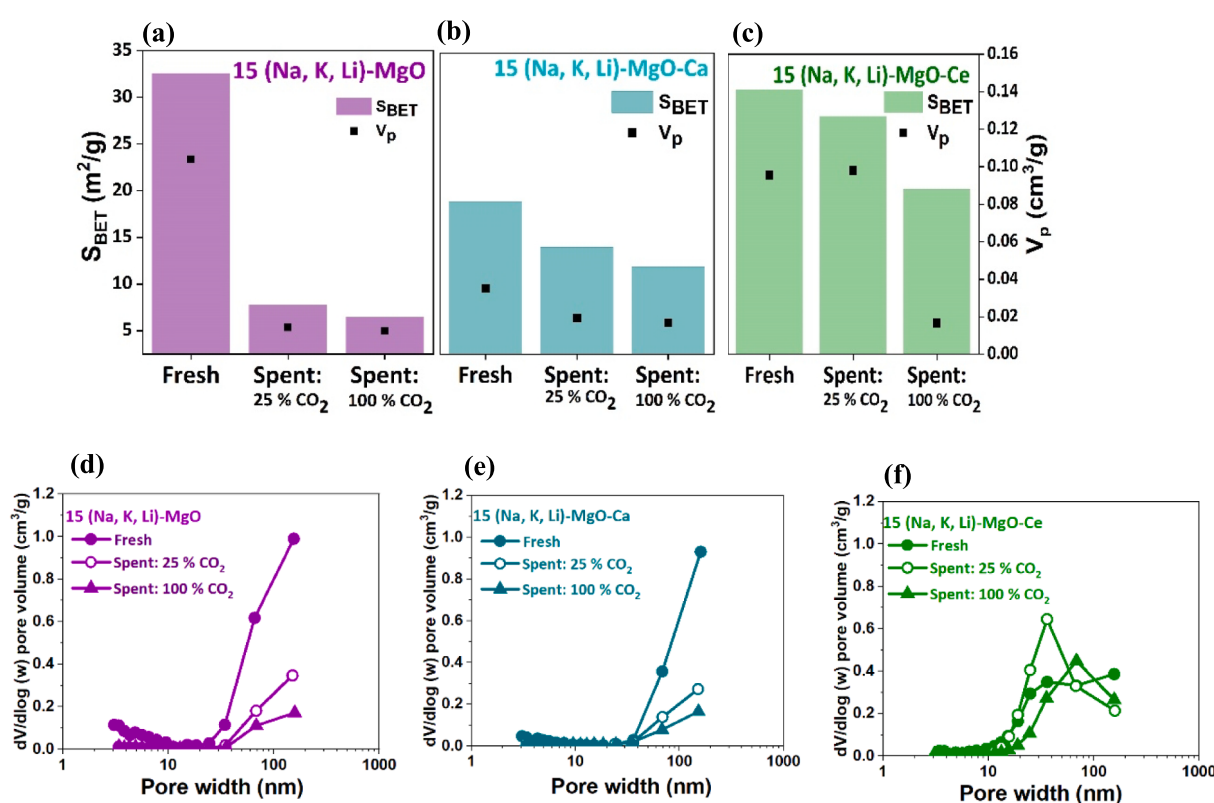
Fig. 10 plots the changes of the MgO crystallite size of the 15 (Na, Li, K)-MgO, 15 (Na, Li, K)-MgO-Ca-SG and 15 (Na, Li, K)-MgO-Ce-SG before (fresh sorbent) and after undergoing 10 carbonation-calcination cycles in a fixed-bed reactor under both carbonation atmospheres, namely, 25

% of CO<sub>2</sub> and 100 % of CO<sub>2</sub>.

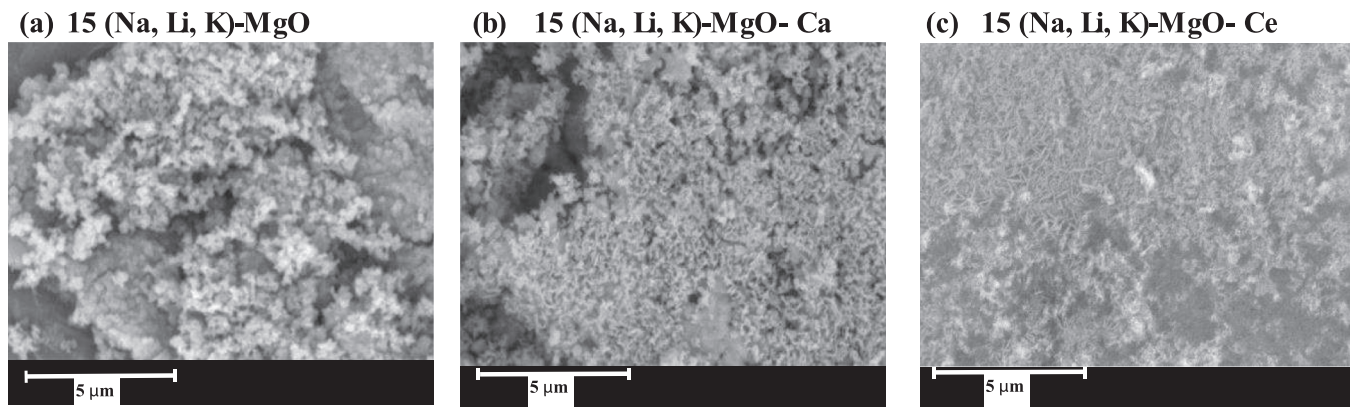
Considering as reference the crystallite size of fresh sorbents, the MgO crystallite size of the unsupported 15 (Na, Li, K)-MgO sorbent was the less stable along the cycles since their size increased 77 % and 73 % under a carbonation atmosphere of 25 % and 100 % of CO<sub>2</sub>, respectively. The lower stability of the unsupported sorbent's crystallites is in line with its higher deactivation along cycles. The 15 (Na, Li, K)-MgO-Ca sorbent registered an increase of the MgO crystallite size of 47 % and 33 % under a carbonation atmosphere of 25 % of CO<sub>2</sub> and of 100 % of CO<sub>2</sub>, respectively. In the other hand, the 15 (Na, Li, K)-MgO-Ce sorbent is presenting more stable crystallites since an increase of 22 % was achieved under an atmosphere of 25 % of CO<sub>2</sub>, and it remained stable under a sorption of 100 % of CO<sub>2</sub>.

Fig. 10 also shows that the MgO crystallites maintain its size a little more stable under a carbonation atmosphere of 100 % of CO<sub>2</sub>, which can be also related with the obtained higher conversions. The reason for this enhanced stability is still unclear but a possible explanation can be the lower thermal conductivity of CO<sub>2</sub> comparatively with air, i.e., 37.8 vs 43.2 ("The Engineering ToolBox," accessed 10.20.22) mW/mK at 280 °C, which can affects the AMS melting behaviour contributing for a lower sintering of crystallites.

After undergoing 10 carbonation-calcination cycles in the fixed-bed unit the sorbents registered a decrease in the S<sub>BET</sub> from fresh to spent on both atmospheres [Fig. 11(a-c)]. Generally, the total pore volume follows the same tendency. Thus, the supported MgO sorbents loose surface area and pore volume during cycling. In addition, the unsupported 15 (Na, Li, K)-MgO shows the highest reduction of S<sub>BET</sub>, suggesting that the addition of support helps the sorbent to keep its surface area closer to that as fresh sorbent. The S<sub>BET</sub> reduction was always higher for sorbents whose carbonation was performed under 100 % of CO<sub>2</sub> than with 25 % of CO<sub>2</sub>, namely, 80 % and 76 % for 15 (Na, Li, K)-MgO, 43 % and 30 % for 15 (Na, Li, K)-MgO-Ca, 38 % and 10 % for 15 (Na, Li, K)-MgO-Ce. The



**Fig. 11.** Properties of 15 (Na, Li, K)-MgO, 15 (Na, Li, K)-MgO-Ca and 15 (Na, Li, K)-MgO-Ce sorbents before (fresh) and after (spent) 10 carbonation-calcination cycles in a fixed bed unit, under a carbonation atmosphere of 25 % or 100 % of CO<sub>2</sub>: (a, b, c) specific surface area (S<sub>BET</sub>) and total pore volume (V<sub>p</sub>), (d, e, f) pore size distribution (PSD) estimated by the BJH desorption.



**Fig. 12.** SEM images of (a) 15 (Na, K, Li)-MgO, (b) 15-(Na, K, Li) MgO-Ca and (c) 15 (Na, K, Li)-MgO-Ce sorbents after 10 carbonation-calcination cycles under a carbonation atmosphere with 100 % of CO<sub>2</sub> in a fixed-bed unit (Scale: 5 μm and magnification: x 30 000).

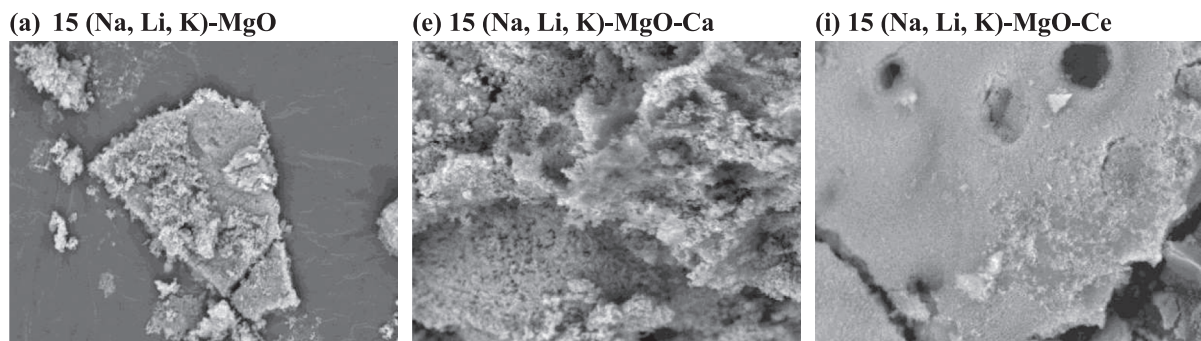


**Fig. 13.** Mapping of SEM images: (a, b, c, d) 15(Na, Li, K)-MgO; (e, f, g, h) 15 (Na, Li, K) MgO-Ca, and (i, j, l, m, n) 15 (Na, Li, K)-MgO-Ce sorbents after 10 carbonation-calcination cycles under a carbonation atmosphere with 100 % of CO<sub>2</sub> in a fixed-bed unit (magnification: x 8 000).

PSD of the 15 (Na, Li, K)-MgO and of the 15 (Na, Li, K)-MgO-Ca are very similar. Both have a PSD highly concentrated in the macropores zone with a decreasing pore volume from fresh to spent under 25 % of CO<sub>2</sub> and, finally, to spent under 100 % of CO<sub>2</sub>. The 15 (Na, Li, K)-MgO-Ce sorbent presents a PSD with higher share of mesoporous, in agreement with the higher S<sub>BET</sub> values.

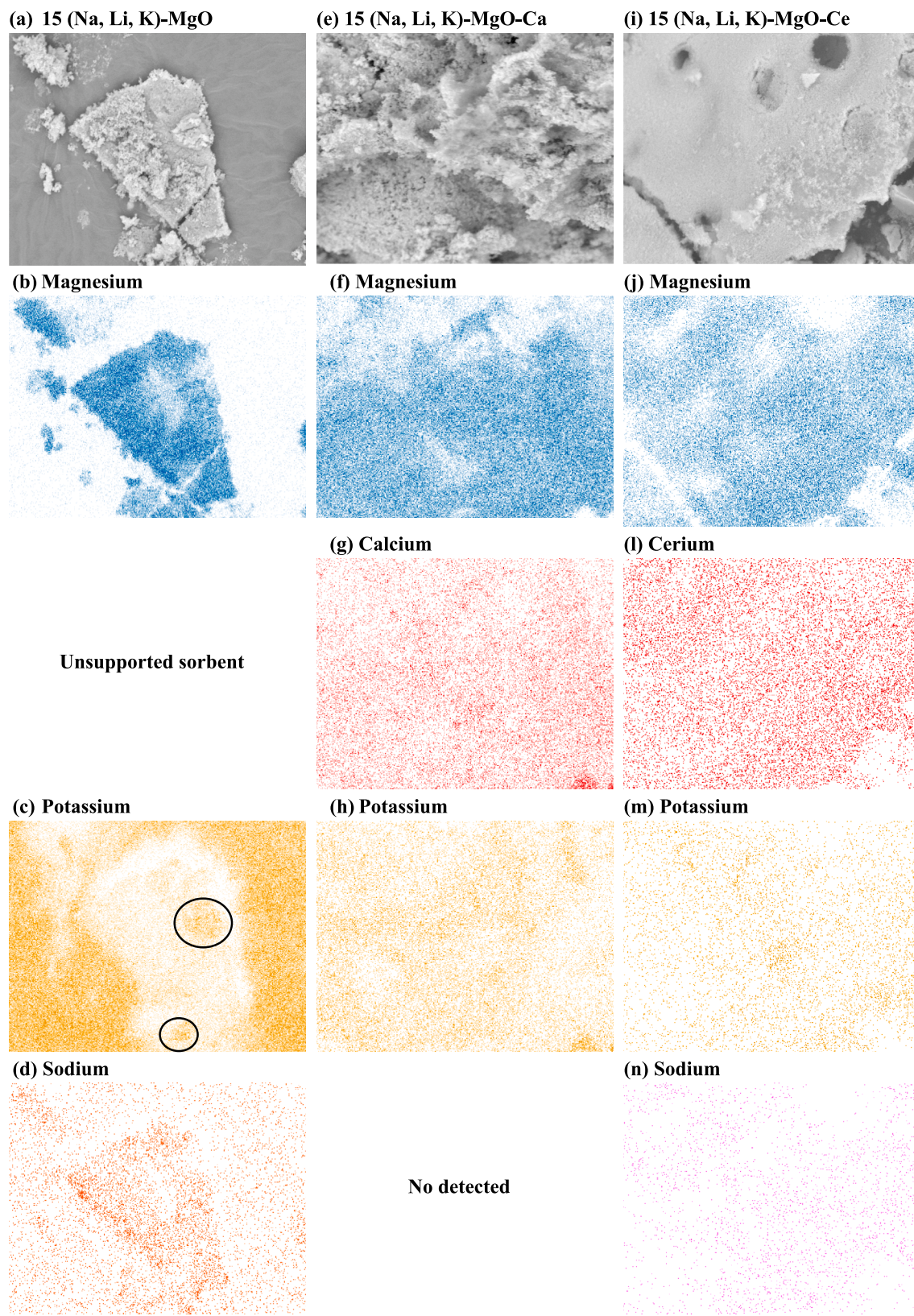
Looking for the carbonation atmosphere effect on the sorbent's crystallite size and S<sub>BET</sub>, it can be stated that a higher CO<sub>2</sub> concentration during the carbonation step contributes for a lower increase of the crystallite size, i.e., lower sintering of MgO crystallite. Yet, lower S<sub>BET</sub> values were achieved for these sorbents. This result confirms that MgO sintering is not the only responsible for the reduction of the surface area and deactivation along cycles, and factors like the nitrates' segregation, as identified above in Fig. 8, can also contribute for the S<sub>BET</sub> reduction. Further studies need to be conducted for a better understanding of the carbonation atmosphere's effect on the sorbents.

To evaluate the sorbents morphology's evolution after undergoing 10 carbonation-calcination cycles in the fixed-bed unit (carbonation atmosphere: 100 % of CO<sub>2</sub>), as well as the distribution of the support (Ca and Ce-based) and of the AMS along the particles, it was carried the SEM analysis. Fig. 12 shows the SEM images of 15 (Na, Li, K)-MgO, 15 (Na, Li, K)-MgO-Ca and 15 (Na, Li, K)-MgO-Ce of sorbents.

SEM images (a) and (b) of Fig. 12 looks similar, but apparently 15 (Na, K, Li)-MgO sorbent presents more compacted zones (lower left corner and upper right corner) than 15 (Na, Li, K)-MgO-Ca, which can be due with a higher sintering degree. In the other hand, the 15 (Na, K, Li)-MgO-Ce sorbents after 10 carbonation-calcination cycles show a more intense presence of thin and long crystals, as well as a slightly grain sintering in the outer surface. Fig. 13 shows the mapping of the main

elements present in specific zones of 15 (Na, Li, K)-MgO, 15 (Na, Li, K)-MgO-Ca and 15 (Na, Li, K)-MgO-Ce of sorbents, acquired by EDS. The evaluation of the elements mapping should be focused only over the particles surface. Calcium and cerium appear to be well-distributed along the MgO particles since no segregation was observed. In supported particles, the potassium distribution along the surface looks to be homogeneous. However, for the unsupported sorbent, an intense signal is observed over the particle (black circles), that can be justified by the occurrence of some sintering associated to the KNO<sub>3</sub>, as already mentioned. The sodium looks to be more concentrated in some zones of the unsupported sorbent than in supported sorbents. In fact, the Na was not detectable in the 15 (Na, Li, K)-MgO-Ca sample, and its signal is very smooth for the 15 (Na, Li, K)-MgO-Ce sorbent, which can be related to the higher dispersion of Na in supported samples, that, in turn, reduces the emitted intensity.

Summarizing, the 15 (Na, Li, K)-MgO sorbent is associated with the highest degree of alkali metal salts aggregation/sintering, which can justify its lower performance in the fixed-bed unit. In the other hand, the Ca and Ce addition contributes for a higher dispersion of AMS on the sorbent, improving their capture capacity, and additionally, the 15 (Na, K, Li)-MgO-Ce sorbent benefits also from its lower particles size. Fig. 14 represents a scheme for the MgO crystallites of unsupported (a, b, c) and supported (d, e, f, g, h, i, j) sorbents doped with an AMS mixture composed by 15 % of NaNO<sub>3</sub>, LiNO<sub>3</sub> and KNO<sub>3</sub> (18/30/52). Before the AMS activation at 450 °C [Fig. 14(a, d, g)] all the sorbents have similar MgO crystallites size (12–13 nm), but it at least duplicates (26–30 nm) after the activation [Fig. 14(b, e, h) and Table 2]. Thus, before the AMS activation, the CaCO<sub>3</sub> and CeO<sub>2</sub> do not have a significant impact on the control of the MgO crystallite size growth, but these supports affect the

**Fig. 13. (continued).**

AMS distribution on the sorbent [Fig. 7, Fig. 8; Fig. 14(b, e, h)]. Both supports contribute positively to the homogeneous distribution of the AMS on the MgO surface, enhancing the sorbent carbonation rate, while in their absence, it is observed the segregation and sintering of AMS,

limiting their role on the MgO dissolution, CO<sub>2</sub> solubility or on both processes. After N carbonation-calcination cycles, the CeO<sub>2</sub> support on the 15(Na,K,Li)-MgO-Ce sorbent can be considered more effective on the MgO crystallite size control than the CaCO<sub>3</sub> support [Fig. 10, Fig. 14(f],

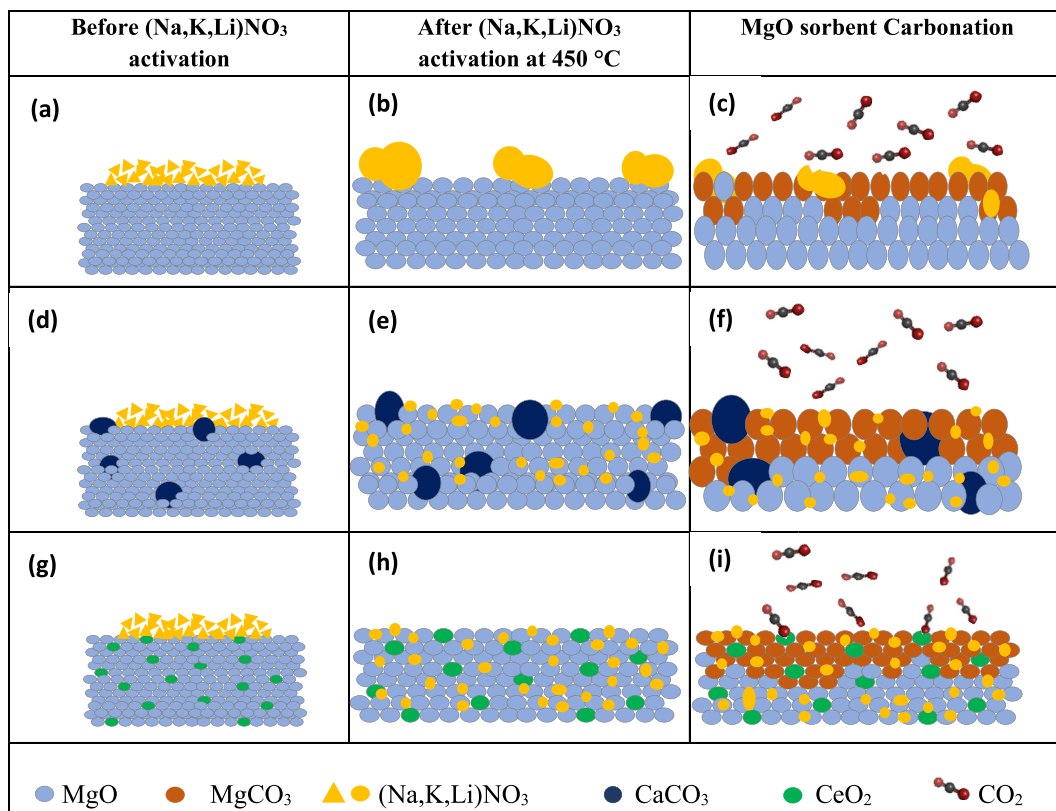


Fig. 14. Scheme of the MgO carbonation promoted by (Na, K, Li)NO<sub>3</sub> with and without CaCO<sub>3</sub> and CeO<sub>2</sub> support.

i)], maybe due to the higher dispersion of its particles on the sorbent. In addition, the high basicity of the CeO<sub>2</sub> (Yu et al., 2018) may increase the sorbent affinity with CO<sub>2</sub>. It means that the surface oxygen on CeO<sub>2</sub> reacted with CO<sub>2</sub> (Fig. 14.i) to form monodentate carbonate, bidentate carbonate, or polydentalate carbonate species (Yoshikawa et al., 2017). For the former species, the desorption temperature occurs approximately at 300 °C, a little higher than the 280 °C used during the carbonation, while for the polydentalate carbonate species the desorption occurs around 500 °C. Since cerium carbonates were not detected on the XRD after the calcination at 400 °C, the formation of polydentalate species did not occur. Despite the identified advantages of the CeO<sub>2</sub> support, the experimental results show that under 25 % of CO<sub>2</sub> at the carbonation atmosphere, the 15(Na, K, Li)-MgO-Ce performs worse than the 15(Na, K, Li)-MgO-Ca. This can be explained by a possible competition between MgO and CeO<sub>2</sub> oxides for CO<sub>2</sub>, that was only overcome under a high CO<sub>2</sub> driving force, as it happened with 100 % CO<sub>2</sub> atmosphere.

#### 4. Conclusions

This work evaluates the efficiency of the sol-gel method in the synthesis of homogeneous and nanosized MgO sorbents, as well as, the effect of Ca and Ce-based supports and the AMS doping on the corresponding sorbents' CO<sub>2</sub> capture capacity. The experiments were carried out in a fixed bed reactor, under a 25 % and 100 % CO<sub>2</sub> carbonation atmosphere, which allow overcoming the TGA experiments' limitations (e.g., high gas-solid ratio) and making a fair judgment on the prediction of the MgO conversion performance.

A higher CO<sub>2</sub> capture capacity was achieved with the 15 (Na, Li, K)-MgO, 15 (Na, Li, K)-MgO-Ca and the 15 (Na, Li, K)-MgO-Ce sorbents for a carbonation atmosphere with 100 % of CO<sub>2</sub> than under an atmosphere of 25 % of CO<sub>2</sub>, which highlights the CO<sub>2</sub> driving force relevance for the process. This was especially observed in the 15 (Na, Li, K)-MgO-Ce sorbent where the MgO conversion is 6 times higher when the CO<sub>2</sub> atmosphere increases from 25 % to 100 %. However, the MgO conversion

to MgCO<sub>3</sub> under an atmosphere of 100 % of CO<sub>2</sub> is not realistic for industrial pre-combustion or post-combustion CO<sub>2</sub> capture conditions. Thus, a more interesting realistic carbonation atmosphere with 25 % of CO<sub>2</sub>, was tested and evaluated, and the 15 (Na, Li, K)-MgO-Ca sorbent shows the best performance, with a conversion 2 times higher than the conversion observed for the case of 15 (Na, Li, K)-MgO and 15 (Na, Li, K)-MgO-Ce sorbents. The lower CO<sub>2</sub> capture capacity of (Na, Li, K)-MgO-Ce sorbents can be explained by a possible competition between MgO and CeO<sub>2</sub> oxides for CO<sub>2</sub>, which was overcome only under a high CO<sub>2</sub> driving force atmosphere. For both carbonation atmospheres, the CO<sub>2</sub> capture capacity was improved for the case of supported sorbents, which can be explained by the reduction of nitrates sintering and segregation, enhanced dispersion of alkali salts on the sorbent and increase of the sorbents' surface area.

Summarizing, the modified MgO-based sorbents proved to be promising materials for CO<sub>2</sub> capture at intermediate temperatures, and their low regeneration temperatures, allow for an energetically competitive process. The AMS segregation is considered as the responsible for the MgO sorbents' deactivation. The supports help increasing the sorbent's activity and stability, but this work shows that they act in different ways, i.e., both contributes to the AMS homogeneous distribution, but affects the MgO sorbents' properties in different ways. For example, CaCO<sub>3</sub> support allows maintaining the sorbent's stability along the carbonation-calcination cycles but has a lower influence on controlling the increase of MgO crystallite size. On the other hand, the CeO<sub>2</sub> potentiates the formation of smaller and stable MgO crystallites, and its higher basicity can have a negative effect on carbon capture when lower CO<sub>2</sub> carbonation partially pressures are used. This result can be useful on further studies, particularly for the evaluation of the synergies between mixed oxides and for the selection of each support molar fraction.

#### CRediT authorship contribution statement

Paula Teixeira: Conceptualization, Formal analysis, Investigation,

Methodology, Validation, Supervision, Writing – original draft, Writing – review & editing. **Patricia Correia:** Investigation, Methodology, Writing – original draft. **Carla I.C. Pinheiro:** Formal analysis, Funding acquisition, Supervision, Writing – review & editing.

## Declaration of competing interest

The authors declare that they have no known competing financial interests or personal relationships that could have appeared to influence the work reported in this paper.

## Data availability

Data will be made available on request.

## Acknowledgements

Authors thank FCT for funding the following projects: Solar-driven Ca-Looping Process for Thermochemical Energy Storage (PTDC/EAM-PEC/32342/2017); Centro de Química Estrutural (UIDB/00100/2020, <https://doi.org/10.54499/UIDB/00100/2020> and UIDP/00100/2020, <https://doi.org/10.54499/UIDP/00100/2020>), and the Institute of Molecular Sciences (LA/P/0056/2020).

## Appendix A. Supplementary data

Supplementary data to this article can be found online at <https://doi.org/10.1016/j.ces.2024.119856>.

## References

- Cavazos, P.A., Hunter-Sellars, E., Iacomi, P., McIntyre, S.R., Danaci, D., Williams, D.R., 2023. Evaluating solid sorbents for CO<sub>2</sub> capture: linking material properties and process efficiency via adsorption performance. *Front. Energy Res.* <https://doi.org/10.3389/fenrg.2023.1167043>.
- Chammingkwan, P., Mai, L.T.T., Ikeda, T., Mohan, P., 2021. Nanostructured magnesium oxide microspheres for efficient carbon dioxide capture. *J. CO<sub>2</sub> Util.* 51 <https://doi.org/10.1016/j.jcou.2021.101652>.
- Chang, R.W., Liou, S.Y.H., Lin, C.J., 2022. Titania spheres with nanochannel-restricted NaNO<sub>2</sub>/MgO for improving cyclic CO<sub>2</sub> adsorption stability. *Environmental Technology (United Kingdom)*. <https://doi.org/10.1080/09593330.2022.2105170>.
- Chen, J., Duan, L., Donat, F., Müller, C.R., 2021. Assessment of the Effect of Process Conditions and Material Characteristics of Alkali Metal Salt Promoted MgO-Based Sorbents on Their CO<sub>2</sub>Capture Performance. *ACS Sustain. Chem. Eng.* 9, 6659–6672. <https://doi.org/10.1021/acssuschemeng.1c00262>.
- Chen, W., Zong, Y., Zhou, Y., Lu, W., Zhang, Y., Qian, J., 2019. The nature of MgO precursor decomposition and pore-forming in hard-templating of porous carbon derived from cotton. *Colloids Surf A Physicochem Eng Asp* 571, 160–167. <https://doi.org/10.1016/j.colsurfa.2019.03.091>.
- Cui, H., Zhang, Q., Hu, Y., Peng, C., Fang, X., Cheng, Z., Galvita, V.V., Zhou, Z., 2018a. Ultrafast and Stable CO<sub>2</sub> Capture Using Alkali Metal Salt-Promoted MgO-CaCO<sub>3</sub> Sorbents. *ACS Appl. Mater. Interfaces* 10, 20611–20620. <https://doi.org/10.1021/acsami.8b05829>.
- Cui, H., Cheng, Z., Zhou, Z., 2020. Unravelling the role of alkaline earth metal carbonates in intermediate temperature CO<sub>2</sub>capture using alkali metal salt-promoted MgO-based sorbents. *J Mater Chem A Mater* 8, 18280–18291. <https://doi.org/10.1039/d0ta06170k>.
- Cui, Z., Gan, J., Fan, J., Xue, Y., Zhang, R., 2018b. Size-Dependent Surface Basicity of Nano-CeO<sub>2</sub> and Desorption Kinetics of CO<sub>2</sub> on Its Surface. *Ind. Eng. Chem. Res.* 57, 10977–10984. <https://doi.org/10.1021/acs.iecr.8b01247>.
- Dal Pozzo, A., Armutlu, A., Rekhitina, M., Abdala, P.M., Müller, C.R., 2019. CO<sub>2</sub> Uptake and Cyclic Stability of MgO-Based CO<sub>2</sub> Sorbents Promoted with Alkali Metal Nitrates and Their Eutectic Mixtures. *ACS Appl Energy Mater* 2, 1295–1307. <https://doi.org/10.1021/acsae.8b01852>.
- Dhoke, C., Zaabout, A., Cloete, S., Amini, S., 2021. Review on reactor configurations for adsorption-based CO<sub>2</sub> capture. *Ind. Eng. Chem. Res.* 60, 3779–3798. <https://doi.org/10.1021/acs.iecr.0c04547>.
- Duong, T.H.Y., Nguyen, T.N., Oanh, H.T., Dang Thi, T.A., Giang, L.N.T., Phuong, H.T., Anh, N.T., Nguyen, B.M., Quang, V.T., Le, G.T., Nguyen, T.V., 2019. Synthesis of Magnesium Oxide Nanoplates and Their Application in Nitrogen Dioxide and Sulfur Dioxide Adsorption. *J. Chem.* 2019 <https://doi.org/10.1155/2019/4376429>.
- The Engineering ToolBox [WWW Document], n.d. URL [https://www.engineeringtoolbox.com/air-properties-viscosity-conductivity-heat-capacity-d\\_1509.html](https://www.engineeringtoolbox.com/air-properties-viscosity-conductivity-heat-capacity-d_1509.html) (accessed 10.20.21).
- Gao, Q., Sun, L., Wang, Q., 2018. Pre-combustion Carbon Dioxide Capture Materials, 1st ed. Royal Society of Chemistry, Beijing.
- Gao, W., Xiao, J., Wang, Q., Li, S., Vasiliades, M.A., Huang, L., Gao, Y., Jiang, Q., Niu, Y., Zhang, B., Liu, Y., He, H., Efstratiou, A.M., 2022. Unravelling the Mechanism of Intermediate-Temperature CO<sub>2</sub> Interaction with Molten-NaNO<sub>3</sub>-Salt-Promoted MgO. *Adv. Mater.* 34 <https://doi.org/10.1002/adma.202106677>.
- Han, K.K., Zhou, Y., Chun, Y., Zhu, J.H., 2012. Efficient MgO-based mesoporous CO<sub>2</sub> trapper and its performance at high temperature. *J. Hazard. Mater.* 203–204, 341–347. <https://doi.org/10.1016/j.jhazmat.2011.12.036>.
- Hanif, A., Sun, M., Tao, Z., Liu, L., Tsang, D.C.W., Gu, Q., Shang, J., 2019. Silica Supported MgO as An Adsorbent for Precombustion CO<sub>2</sub> Capture. *ACS Appl Nano Mater* 2, 6565–6574. <https://doi.org/10.1021/acsnano.9b01481>.
- Harada, T., Simeon, F., Hamad, E.Z., Hatton, T.A., 2015. Alkali metal nitrate-promoted high-capacity MgO adsorbents for regenerable CO<sub>2</sub> capture at moderate temperatures. *Chem. Mater.* 27, 1943–1949. <https://doi.org/10.1021/cm503295g>.
- Hu, Y., Guo, Y., Sun, J., Li, H., Liu, W., 2019. Progress in MgO sorbents for cyclic CO<sub>2</sub> capture: A comprehensive review. *J Mater Chem A Mater* 7, 20103–20120. <https://doi.org/10.1039/c9ta06930e>.
- IEA, 2020. Technology Perspectives Energy Special Report on Carbon Capture Utilisation and Storage CCUS in clean energy transitions.
- IEA, 2021. Net Zero by 2050 - A Roadmap for the Global Energy Sector.
- Jeevanandam, J., San Chan, Y., Danquah, M.K., 2019. Effect of Gelling Agent and Calcination Temperature in Sol-Gel Synthesized MgO Nanoparticles. *Prot. Met. Phys. Chem* 55, 288–301. <https://doi.org/10.1134/S2070205119020114>.
- Jin, S., Ho, K., Lee, C.H., 2018. Facile synthesis of hierarchically porous MgO sorbent doped with CaCO<sub>3</sub> for fast CO<sub>2</sub> capture in rapid intermediate temperature swing sorption. *Chem. Eng. J.* 334, 1605–1613. <https://doi.org/10.1016/j.cej.2017.11.095>.
- Jin, S., Ko, K.J., Lee, C.H., 2019. Direct formation of hierarchically porous MgO-based sorbent bead for enhanced CO<sub>2</sub> capture at intermediate temperatures. *Chem. Eng. J.* 371, 64–77. <https://doi.org/10.1016/j.cej.2019.04.020>.
- Jo, S.I., An, Y.I., Kim, K.Y., Choi, S.Y., Kwak, J.S., Oh, K.R., Kwon, Y.U., 2017. Mechanisms of absorption and desorption of CO<sub>2</sub> by molten NaNO<sub>3</sub>-promoted MgO. *PCCP* 19, 6224–6232. <https://doi.org/10.1039/c9cp07787k>.
- Kwak, J.S., Oh, K.R., Kim, K.Y., Lee, J.M., Kwon, Y.U., 2019. CO<sub>2</sub> absorption and desorption characteristics of MgO-based absorbent promoted by triple eutectic alkali carbonate. *PCCP* 21, 20805–20813. <https://doi.org/10.1039/c9cp03258d>.
- Landuyt, A., Kumar, P.V., Yuwono, J.A., Bork, A.H., Donat, F., Abdala, P.M., Müller, C.R., 2022. Uncovering the CO<sub>2</sub>Capture Mechanism of NaNO<sub>3</sub>-Promoted MgO by 18O Isotope Labeling. *J. Am. Chem. Soc.* 2, 2731–2741. <https://doi.org/10.1021/jacsau.2c00461>.
- Papalas, T., Polychronidis, I., Antzuras, A.N., Lemonidou, A.A., 2021b. Enhancing the intermediate-temperature CO<sub>2</sub> capture efficiency of mineral MgO via molten alkali nitrates and CaCO<sub>3</sub>: Characterization and sorption mechanism. *J. CO<sub>2</sub> Util.* 50 <https://doi.org/10.1016/j.jcou.2021.101605>.
- Papalas, T., Antzuras, A.N., Lemonidou, A.A., 2021a. Magnesite-derived MgO promoted with molten salts and limestone as highly-efficient CO<sub>2</sub> sorbent. *J. CO<sub>2</sub> Util.* 53, 101725 <https://doi.org/10.1016/j.jcou.2021.101725>.
- Park, S.J., Kim, Y., Jones, C.W., 2020. NaNO<sub>3</sub>-Promoted Mesoporous MgO for High-Capacity CO<sub>2</sub> Capture from Simulated Flue Gas with Isothermal Regeneration. *ChemSusChem* 13, 2988–2995. <https://doi.org/10.1002/cssc.202000259>.
- Reddy, P., Sadasivuni, K., Abdulla, 2021. Carbon dioxide adsorption based on porous materials. *RSC Adv.* <https://doi.org/10.1039/dra10902a>.
- Ruhaimi, A.H., Aziz, M.A.A., Jalil, A.A., 2021. Magnesium oxide-based adsorbents for carbon dioxide capture: Current progress and future opportunities. *J. CO<sub>2</sub> Util.* <https://doi.org/10.1016/j.jcou.2020.101357>.
- Salman, K.D., Abbas, H.H., Aljawad, H.A., 2021. Synthesis and characterization of MgO nanoparticle via microwave and sol-gel methods. *J. Phys. Conf. Ser.* 1973 <https://doi.org/10.1088/1742-6596/1973/1/012104>.
- Teixeira, P., Hipólito, J., Fernandes, A., Ribeiro, F., Pinheiro, C.I.C., 2019. Tailoring Synthetic Sol-Gel CaO Sorbents with High Reactivity or High Stability for Ca-Looping CO<sub>2</sub> Capture. *Ind. Eng. Chem. Res.* 58, 8484–8494. <https://doi.org/10.1021/acs.iecr.8b05311>.
- Teixeira, P., Bacariza, C., Correia, P., Pinheiro, C.I.C., Cabrita, I., 2022. Hydrogen Production with In Situ CO<sub>2</sub> Capture at High and Medium Temperatures Using Solid Sorbents. *Energies (basel)*. <https://doi.org/10.3390/en15114039>.
- Thommes, M., Kaneko, K., Neimark, A.V., Olivier, J.P., Rodriguez-Reinoso, F., Rouquerol, J., Sing, K.S.W., 2015. Physisorption of gases, with special reference to the evaluation of surface area and pore size distribution (IUPAC Technical Report). *Pure Appl. Chem.* 87, 1051–1069. <https://doi.org/10.1515/pac-2014-1117>.
- Vu, A.T., Park, Y., Jeon, P.R., Lee, C.H., 2014. Mesoporous MgO sorbent promoted with KNO<sub>3</sub> for CO<sub>2</sub> capture at intermediate temperatures. *Chem. Eng. J.* 258, 254–264. <https://doi.org/10.1016/j.cej.2014.07.088>.
- Wang, Q., Gao, W., 2018. MgO-based Intermediate-temperature CO<sub>2</sub> Adsorbents. In: Wang, Q. (Ed.), *Pre-Combustion Carbon Dioxide Capture Materials*. Royal Society of Chemistry, Beijing.
- Wang, J., Li, M., Lu, P., Ning, P., Wang, Q., 2020. Kinetic study of CO<sub>2</sub> capture on ternary nitrates modified MgO with different precursor and morphology. *Chem. Eng. J.* 392 <https://doi.org/10.1016/j.cej.2019.123752>.
- Xiong, J., Bo, K., Li, R., Feng, Y., 2021. Promotion effect of Ce doping on MgO-based adsorbents for CO<sub>2</sub> adsorption performances. *Ferroelectrics* 581, 209–220. <https://doi.org/10.1080/00150193.2021.1905744>.
- Yang, X., Zhao, L., Li, X., Xiao, Y., 2018. Magnesium Oxide-Based Absorbents for CO<sub>2</sub> Capture at Medium Temperature. *Curr Pollut Rep* 4, 13–22. <https://doi.org/10.1007/s40726-018-0074-z>.
- Yoshikawa, K., Kaneeda, M., Nakamura, H., 2017. Development of Novel CeO<sub>2</sub>-based CO<sub>2</sub> adsorbent and analysis on its CO<sub>2</sub> adsorption and desorption mechanism, in:

Energy Procedia. Elsevier Ltd, pp. 2481–2487. <https://doi.org/10.1016/j,egypro.2017.03.1400>.

Yu, H., Wang, X., Shu, Z., Fujii, M., Song, C., 2018. Al<sub>2</sub>O<sub>3</sub> and CeO<sub>2</sub>-promoted MgO sorbents for CO<sub>2</sub> capture at moderate temperatures. *Front. Chem. Sci. Eng.* 12, 83–93. <https://doi.org/10.1007/s11705-017-1691-6>.

Zhang, K., Li, X.S., Li, W.Z., Rohatgi, A., Duan, Y., Singh, P., Li, L., King, D.L., 2014. Phase Transfer-Catalyzed Fast CO<sub>2</sub> Absorption by MgO-Based Absorbents with High Cycling Capacity. *Adv. Mater. Interfaces* 1, 1–6. <https://doi.org/10.1002/admi.201400030>.